Loading Rate-Dependent Mechanical Properties of Bulk Two-Phase Nanocrystalline Al-Pb Alloys Studied by Nanoindentation

Article *in* Metallurgical and Materials Transactions A · October 2014

DOI: 10.1007/s11661-014-2425-8

CITATIONS
8

READS
211

6 authors, including:

Sreedevi Varam
National Institute of Technology, Warangal
7 PUBLICATIONS **48** CITATIONS
SEE PROFILE

Koteswararao V. Rajulapati
University of Hyderabad
69 PUBLICATIONS **1,066** CITATIONS
SEE PROFILE

Kota bhanu sankara rao
University of Hyderabad
272 PUBLICATIONS **6,133** CITATIONS
SEE PROFILE

Ronald Scattergood
North Carolina State University
208 PUBLICATIONS **7,698** CITATIONS
SEE PROFILE

Loading Rate-Dependent Mechanical Properties of Bulk Two-Phase Nanocrystalline Al-Pb Alloys Studied by Nanoindentation

SREEDEVI VARAM, KOTESWARARAO V. RAJULAPATI, K. BHANU SANKARA RAO, RONALD O. SCATTERGOOD, KORUKONDA L. MURTY, and CARL C. KOCH

Bulk samples (dia. = 20 mm) of various nanocrystalline (nc) Al-Pb alloys with Pb content varying from 1 to 4 at. pct are fabricated using spark plasma sintering of ball-milled powders. Al matrix in Al-2 at. pct Pb alloy had a grain size of 53 nm, and Pb particle size was 6 ± 2 nm. High angle annular dark-field image obtained in STEM mode of TEM indicates the presence of Pb along the nc Al grain boundaries as well as dispersion of smaller Pb particles in the intragranular regions. Hardness studies are carried out using microindentation and nanoindentation with load varying over three orders of magnitude (100 − 0.1 g). Microindentation yielded slightly smaller hardness values in comparison to nanoindentation possibly because of indentation size effect. Nevertheless both microindentation and nanoindentation resulted in the same trend of hardness for various nc Al-Pb alloys. Hardness of Al-Pb alloys increased with increase in Pb content up to the additions of 2 at. pct Pb, beyond that the hardness is decreased for higher Pb additions of 3 and 4 pct. The initial hardening behavior is explained based on the Orowan particle strengthening. Strain rate sensitivity (SRS) has increased with increase in Pb content reaching a value of 0.1 for Al-4 at. pct Pb alloy. Activation volumes measured are between 2.84 and 6.15 b^3. Higher SRS and lower activation volume suggest that grain boundary-mediated processes are controlling the deformation characteristics.

DOI: 10.1007/s11661-014-2425-8

I. INTRODUCTION

THE deformation behavior of nanocrystalline materials has been fascinating as it distinctly differs from that of coarse-grained materials.[1,2] In structural materials of engineering importance with micron sized characteristic length scales (grain size) in three dimensions, mobile dislocations located in the interiors of the grains play a dominant role, governing the plasticity.[3] In single phase materials, as the grain size is refined to less than 100 nm, the larger fractions of grain boundaries and other interfaces also will contribute to the plastic deformation in a significant way.[4–9] As grain size (d) is reduced, the strength increases in polycrystalline solids following Hall–Petch relation.[10,11] However, when the grain size approaches ≤100 nm, the Hall–Petch line will have a different slope, than that in 100 nm ≤ d ≤ 1000 nm range, albeit a positive number. With grain size further decreasing to about 10 nm, the Hall–Petch line exhibited a negative slope suggesting that the strength decreases in materials with these very fine grain sizes approaching the amorphous limit.[4] This is termed as Inverse Hall–Petch effect.[12] The interesting and superior mechanical properties of nanocrystalline materials have thrown a grand challenge to the scientific community in the form of several uncertainties and unanswered questions, while unfolding the underlying deformation mechanisms.[5] Finer grain size yielded higher strength values in nanocrystalline single-phase materials, but at the expense of ductility.[13] Therefore, acceptable ductility levels should also be available along with strength in these materials for potential structural applications. Strain rate sensitivity (SRS) and activation volume are important parameters in a plastic deformation process.[14] SRS is a qualitative indicator of ductility of a given material, with higher SRS value means more ductility.[15] While suggesting strategies to improve ductility of nanocrystalline materials, Koch[16] indicated that incorporation of a second phase could delay the onset of localized deformation under tensile loading conditions. Although extensive research investigations have been carried out to explore the mechanical behavior of various single-phase nc materials, studies that address the influence of a nano-sized second phase dispersions in a nanocrystalline matrix with an average grain size less than 100 nm are very limited as of today.[17] Hardness/strength, SRS and activation volume of several single-phase materials with nanocrystalline features have been reported. Scientific attention is

SREEDEVI VARAM, Doctoral Student, and KOTESWARARAO V. RAJULAPATI, Assistant Professor, are with the School of Engineering Sciences and Technology, University of Hyderabad, Gachibowli, Hyderabad 500046, India. Contact e-mail: kvrse@uohyd.ernet.in K. BHANU SANKARA RAO, Ministry of Steel Chair (Govt. of India), is with MGIT, Hyderabad. RONALD O. SCATTERGOOD, KORUKONDA L. MURTY, and CARL C. KOCH, Professors, are with the Department of Materials Science and Engineering, North Carolina State University, Raleigh, NC 27695-7907, USA.

Manuscript submitted February 21, 2014.
Article published online July 11, 2014

needed to understand the SRS and activation volume involved during the deformation of two-phase nanocrystalline materials.

Therefore, motivated by the current status on deformation behavior of nanocrystalline materials especially two-phase materials as mentioned above, attempts have been made to explore the role of a second phase on the mechanical properties (hardness, strain rate sensitivity, and activation volume) of a nanocrystalline matrix. Al-Pb system was chosen as a model system as Al and Pb have a misfit of about 22 pct in size, and they are immiscible both in liquid state as well as solid state. Bulk Al-Pb nanocomposites with varied Pb concentrations are fabricated using a combination of high-energy ball milling and spark plasma sintering (SPS). Mechanical properties are evaluated using Vickers microindentation as well as nanoindentation. Nanoindentation was performed at different peak loads and loading rates to calculate SRS and activation volume associated with the deformation process.

II. MATERIALS AND METHODS

Al powder (99.0 pct purity, +200 mesh, S-D Fine Chemicals Limited) and Pb powder (99.9 pct purity, −200 mesh, Alfa Aesar) were used as raw materials and SPEX 8000D Mixer/Mill was used to produce nanocrystalline powders at room temperature. The processing was performed using hardened steel milling media at a ball to powder weight ratio of 5:1. Milling was done for 50 hours under high purity argon atmosphere to protect the freshly fractured surfaces during milling from contamination. To prevent cold welding during milling, 1.5 wt pct stearic acid was added as surfactant. Various compositions were prepared with Pb content varying from 0 to 4 at. pct. Handling of powders throughout the milling process was done in a glove box. The as-milled powders are compacted into 20-mm diameter disks by applying a uni-axial pressure of 600MPa at room temperature. The compacted samples were sintered at 573 K (300 °C) using SPS. Structural characterization of the alloy powders as well as sintered products was carried out by X-ray diffraction (XRD) and transmission electron microscopy (TEM). XRD investigations were carried out using BRUKER D8 ADVANCE X-ray diffractometer with Cu K-α radiation of wavelength 1.54056 Å at a scan speed of 3 s/step, a step size being 0.05 deg. Thin electron-transparent samples were prepared by ion-beam milling using Gatan's precision ion polishing system (PIPS) for TEM observations. TEM analysis was done using Tecnai FEI G2 S-Twin instrument with an applied voltage of 200 keV. Bulk samples were metallographically polished to a mirror-like surface prior to microindentation and nanoindentation testing. Microhardness measurements were carried out using Vickers microindenter (Omnitech-MVH-Sauto with 10 seconds dwell time) at various loads ranging from 25 to 100 g. Each datum point is an average of 10 indentations performed under identical conditions. Nanoindentation was carried out at various peak loads (1000, 2000, and 4500 μN) and loading rates (100, 500, and 1000 μN/s) using Hysitron TI950 Triboindenter. At a given set of load and loading rate, 49 indentations (7 × 7 matrix) were made to have a meaningful statistical analysis of the data. Loading rate divided by the peak load applied is considered as strain rate. Hence, for a peak load of 1000 μN, the strain rates are 0.1, 0.5 and 1 s^{-1}, respectively.

III. RESULTS AND DISCUSSION

A. *Structural Details of Nanocrystalline Al-Pb Alloys*

X-ray diffractograms of various Al-Pb alloys in as-milled condition are shown in Figure 1. It is clear that the reflections corresponding to only Al and Pb are present, ruling out the formation of any solid solution or meta-stable phase during ball milling. The precise lattice parameter of Al in all Al-Pb alloys, calculated using Nelson–Riley extrapolation analysis,[18] yielded a value of 4.0481 ± 0.0005 Å against standard literature value of 4.0495 Å indicating that there is no considerable change in the lattice parameter of Al and the difference is within the instrumental error. Grain size of aluminum was calculated using Scherrer equation[19] after accounting for instrumental broadening. The grain size of aluminum in all the Al-Pb alloys is about 45 ± 6 nm. Although, Pb content was varied between 0 and 4 at. pct in various alloys, the grain size of aluminum matrix remains the same suggesting that Pb is not influencing the grain size in nanocrystalline Al-Pb system. This is in well agreement with earlier reports on nanocrystalline Al-Pb alloys prepared using ball milling.[20,21] The microstructural features of Al-2 at. pct Pb alloy obtained using TEM are shown Figures 2(a) and (b) and 3. Figure 2(a) is the bright field image, Figure 2(b) is the dark-field image with diffraction pattern in the inset, and Figure 3 is the histogram showing grain size distribution of Al in Al-2 at. pct Pb alloy in as-milled condition. Grain size calculated using linear intercept method from 200 grains is about

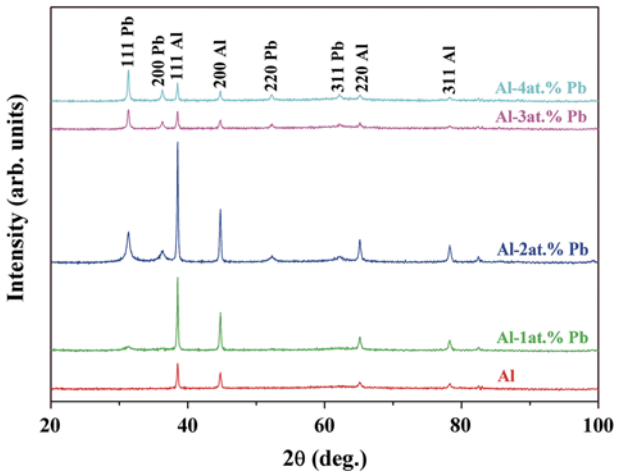

Fig. 1—X-ray diffractograms of ball-milled Al-Pb nanocomposites showing a two-phase mixture of Al and Pb.

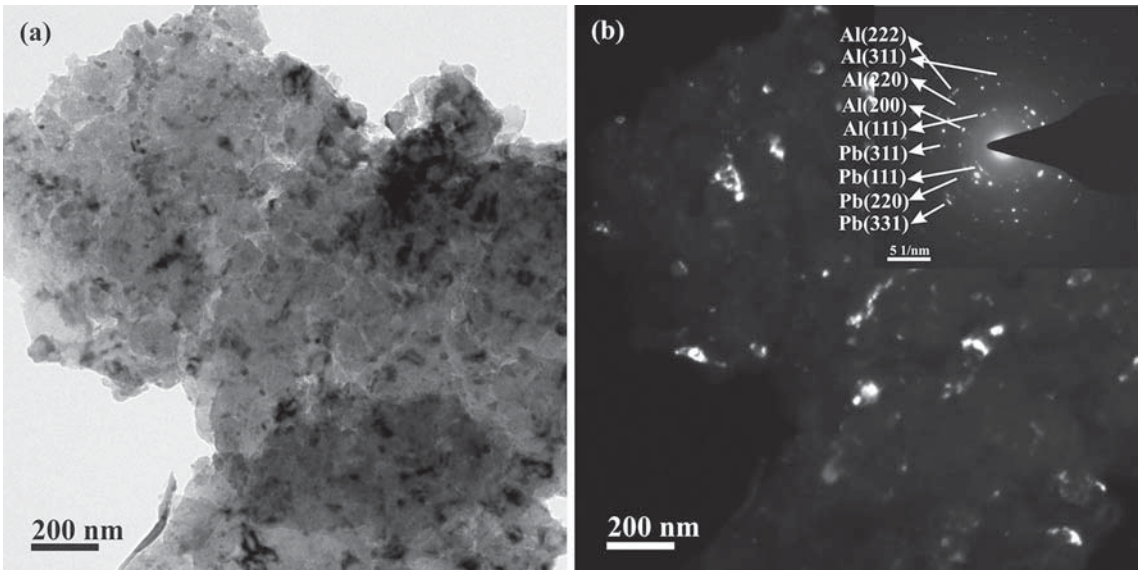

Fig. 2—(*a*) Bright field and (*b*) dark-field transmission electron micrographs, and the corresponding diffraction pattern in the inset of Al-2 at. pct Pb powder milled for 50 h.

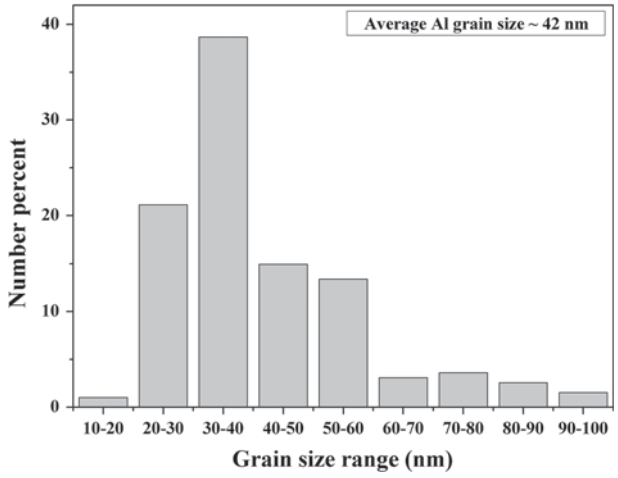

Fig. 3—The grain size distribution of Al in Al-2 at. pct Pb powder milled for 50 h.

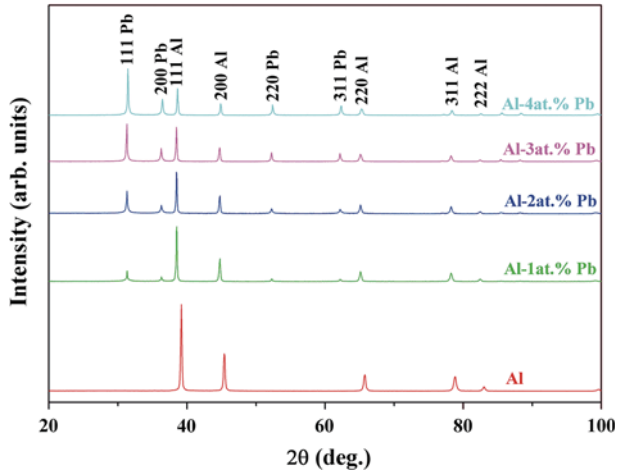

Fig. 4—X-ray diffractograms of sintered Al-Pb nanocomposites showing two-phase mixture of Al and Pb.

42 (±17) nm. Indexing of the diffraction pattern (Figure 2(b) inset) shows that reflections corresponding to only Al and Pb are present which is consistent with XRD analysis (Figure 1).

To study the bulk mechanical behavior of these Al-Pb nanocomposites, milled powders are compacted using SPS at 573 K (300 °C). X-ray diffractograms of various Al-Pb alloys recorded post-sintering are given in Figure 4. From Figure 4, it is evident that only two-phase mixtures of Al and Pb are present in these alloys. Microstructural features of Al-2 at. pct Pb alloy obtained using TEM are shown in Figures 5(a) and (b) and Figure 6. Figure 5(a) is the bright field image, Figure 5(b) is the dark-field image with diffraction pattern in the inset, and Figure 6 is the histogram showing grain size distribution of Al in Al-2 at. pct Pb alloy in as-sintered condition. Grain size calculated from about 200 grains using linear intercept method is 53 (±18) nm. Grain size of Al has increased from 42 to 53 nm during SPS. Even after exposing these alloys to homologous temperature (T/T_M) of 0.6, there was no significant grain growth. This could be because of Pb present in the aluminum grain boundaries. Pb might be pinning the grain boundaries and affecting their mobility at elevated temperatures and in turn resulting in minimum grain growth. Al-Pb alloys in the present study resulted in 92 pct density after SPS. High-resolution TEM image shown in Figure 7 infers that the Pb particles (circled) are about 6-8 nm in diameter dispersed in aluminum matrix. To further elucidate the presence and distribution of Pb, Z-contrast imaging was employed in scanning transmission electron mode (STEM) in TEM. Z-contrast imaging aids in identifying the presence of two different elements/phases with wide variation in their atomic number as the intensity, I scales as Z^2 (*i.e.*, $I \propto Z^2$), where Z is the atomic number.[22]

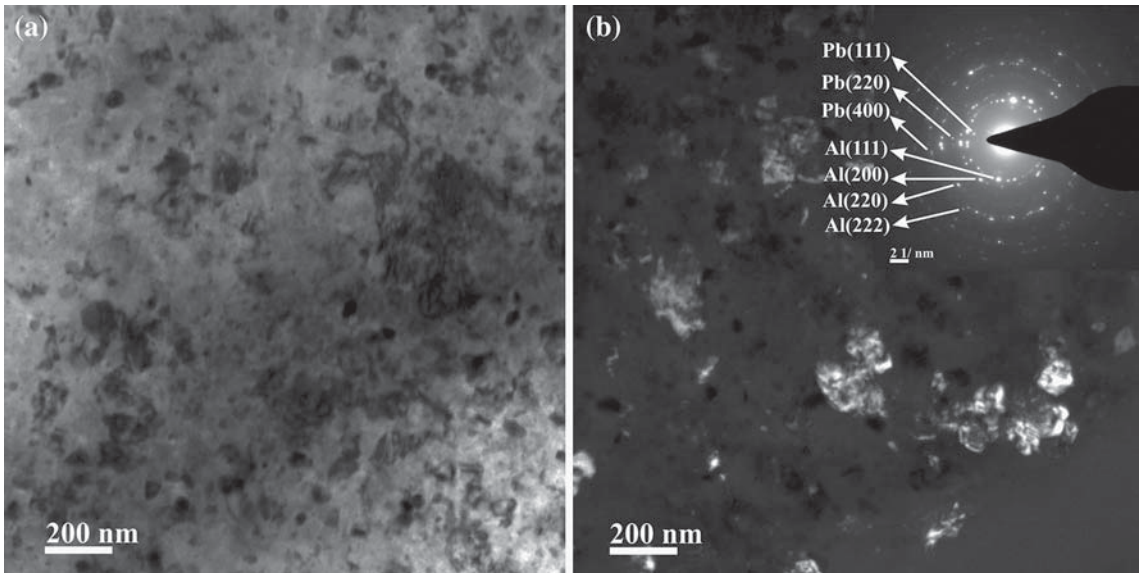

Fig. 5—Bright field and dark-field transmission electron micrographs ((*a*) and (*b*)) and the corresponding diffraction pattern (inset of (*b*)) of sintered Al-2 at. pct Pb alloy.

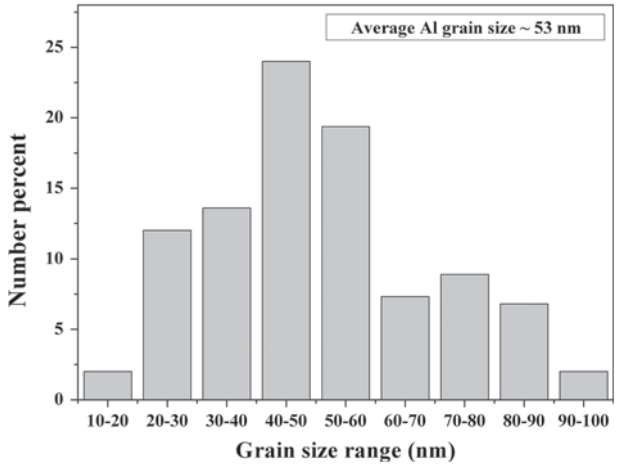

Fig. 6—The histogram showing the distribution of Al grain size in sintered Al-2 at. pct Pb alloy.

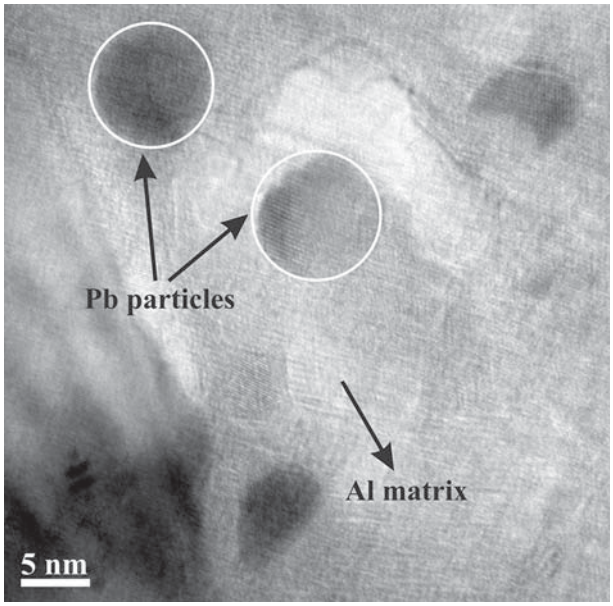

Fig. 7—High-resolution transmission electron micrograph of sintered Al-2 at. pct Pb sample indicating Pb particles of ~6 nm dispersed in Al matrix.

Figure 8 is the *Z*-contrast image obtained from Al-2 at. pct Pb sample, and it is clear that the region that is brighter in contrast belongs to Pb phase. It is evident that Pb is segregating to aluminum grain boundaries (shown with arrows) and also dispersed as fine particles within the grain. The distribution of Pb particle size is shown in Figure 9, and the average Pb particle size assumes to be 6 (±2) nm. Therefore, in summary, nanocrystalline aluminum with an average grain size of 53 nm contains Pb along its grain boundaries as well as dispersion of Pb particles within the grain.

B. *Hardness Measurements Using Microindentation and Nanoindentation*

Microhardness measurements are made at various loads in the range of 25 to 100 g, and the obtained data are shown in Figure 10. Nanoindentation data obtained at various loads in the range of 0.1 to 0.45 g is also shown in Figure 10 for comparison purpose. From Figure 10, it is evident that as Pb content is increased, hardness of these composites also increases by about 7 to 15 pct up to 2 at. pct Pb additions, whereas the addition of Pb above 2 at. pct, resulted in decrease in hardness. Microhardness values measured for a given composite are always lower than that of nanohardeness values. This could be because of indentation size effect (ISE) [24–32] as the loads employed in nanoindentation (0.1 g) are almost about three orders of magnitude lower

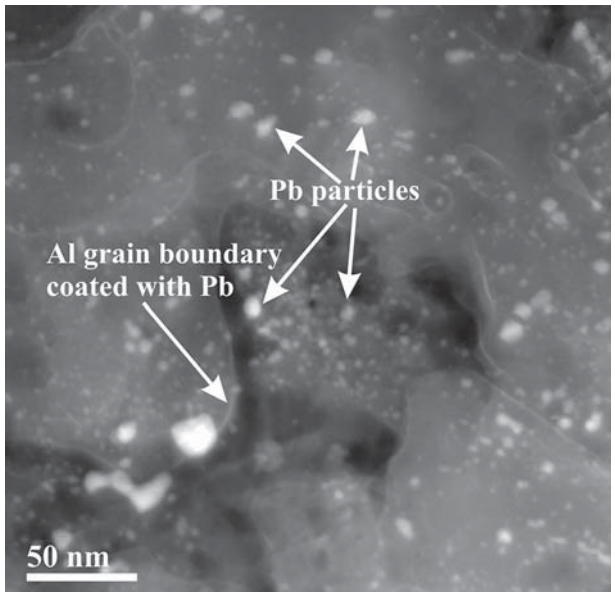

Fig. 8—High angle annular dark-field image of sintered Al-2 at. pct Pb sample. The arrow indicates the nc Al grain boundary decorated with Pb phase. The smaller Pb particles are also seen in the grain interior.

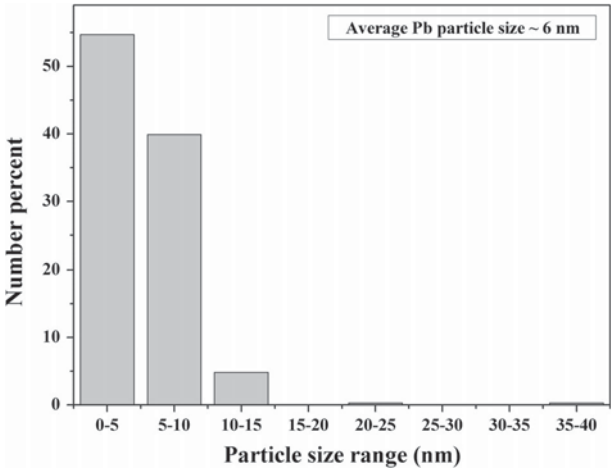

Fig. 9—Size distribution plot of Pb particles obtained from high angle annular dark-field image (Fig. 8) of sintered Al-2 at. pct Pb sample showing an average particle size of ~6 nm.

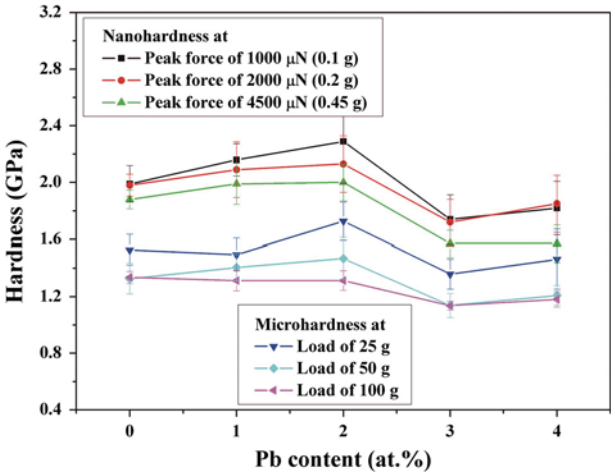

Fig. 10—Variation of hardness with increasing Pb content of Al-Pb nanocomposites obtained by performing microhardness testing in the load range of 25 to 100 g. The hardness data obtained using nanoindentation at different peak forces (1000, 2000, and 4500 μN) with a loading rate of 500 μN/s is also shown in the same plot.

than those in microindentation (100 g). This observation is also in agreement with various studies performed on various material systems using both microindentation and nanoindentation.[24] Various reasons such as confinement of deformation only to small volumes, elastic recovery after indentation at small loads, indenter-sample friction/surface effects, strain gradient plasticity, *etc*., were attributed to the ISE as summarized in Reference 25. However, there is no clear understanding and/or universal agreement among the research community for the ISE observed in various materials. In the current study, even though there is an indentation size effect, the trend in hardness variation among various alloys as well as at various loads is same for both microindentation and nanoindentation data (Figure 10). In addition, it is to be noted that, in order to test the reasonable amount of materials, microindentation as well as nanoindentation testing was carried out at various loads and loading rates thus sampling reasonably larger volume during deformation so that the bulk behavior of these two-phase nanomaterials could be understood.

Since there is a size mismatch of about 22 pct among Al and Pb atoms, it is possible that Pb atoms initially (*i.e*., at lower concentrations) segregate to Al grain boundaries. As Pb content is increased, once Al grain boundaries get saturated with Pb atom segregates, excess Pb will be available inside the grains as small Pb particles as it is clearly evident from the *Z*-contrast image of Al-2 at. pct Pb alloy in the present investigation (Figures 7 and 8). In the earlier experimental work,[20] average grain size of the nc Al matrix was reported to be 28 nm. Therefore, in this case, to have a monolayer coating along nc Al grain boundaries, a Pb volume fraction of about 1.4 pct is required as per $f = 1/(1 + 2.55d)$,[23] where f is volume fraction and d is grain size. In the current study (d = 53 nm), only 0.7 vol pct is sufficient to saturate the grain boundaries. The remaining Pb is expected to be present inside the grains in the form of particles. In addition, these small particles become larger in size with further increase in Pb content.[21] Therefore, contributions to the observed mechanical behavior in the current study come from the following factors: (i) aluminum matrix grain size (53 nm), (ii) Pb atom segregates present in nc Al grain boundary (Figure 8), and (iii) size and distribution of Pb particles present in the intra-granular regions (Figure 8).

Experimental studies on different Al-Pb alloys with Pb content varying between 0.1 and 1.0 at. pct carried out by Rajulapati *et al*.[20] showed a precipitous softening effect as the Pb content is increased. Al-1 at. pct Pb sample with Al matrix grain size of 28 nm had a lower

hardness value by about 35 pct in comparison to nc Al with a similar grain size. The dramatic reduction in hardness was attributed to the presence of Pb atom segregates in nc Al grain boundaries and thereby making lattice defect generation easier during deformation. Subsequently, supporting their results, Jang *et al.*[23] also noticed decrease in yield stress with increased Pb content using Monte Carlo and Molecular Dynamics simulations on Al-Pb alloys containing 1, 2, and 3 at. pct Pb. But, this decrease in yield strength observed is less dramatic than the softening observed experimentally earlier.[20] Their simulations also showed that Pb atoms segregate to Al grain boundaries and this segregation resulted in lower yield stresses. Prior to these two studies, investigations by Sheng *et al.*[21] on Al-Pb nanocomposites indicated that small amounts of Pb, in the form of nano particles may strengthen the Al matrix.

In order to have a detailed understanding on deformation mechanisms that are being operated in these various two-phase Al-Pb alloys, the model equations developed by Scattergood *et al.*[33] have been considered. These model equations for Hall–Petch strengthening due to decrease in grain size and Orowan particle strengthening in nanocrystalline alloys are as follows

$$H_{\mathrm{HP}} = H_{\mathrm{o}} + \frac{3Gb}{\pi}\frac{1}{d}\ln\frac{d}{r_{\mathrm{o}}} \qquad [1]$$

$$\Delta H_{\mathrm{p}} = \frac{3Gb}{\pi}\left\{\frac{1}{d\left(1-\sqrt{f}\right)}\left[\frac{d\sqrt{f}}{D}\ln\frac{D}{r_{\mathrm{o}}} + \ln d\right] - \frac{1}{d}\ln\frac{d}{r_{\mathrm{o}}}\right\}, \qquad [2]$$

where H_{HP} in Eq. [1] is the hardening due to grain size d of matrix, H_{o} is a free parameter, G is the shear modulus, b is the Burgers vector and r_{o} is the core-cutoff distance in the dislocation line energy. Hardening increment due to Orowan particle strengthening is given by ΔH_{p} in Eq. [2] where f and D are the volume fraction and particle size of second-phase particles having $D < d$. Based on these equations the hardness values of the Al-Pb alloys are estimated using G = 26.1 GPa, b = 0.286 nm, r_{o} = 1 nm, d_{Al} = 53 nm, D = 6 nm and H_{Al} = 1.27 GPa for Al matrix. Figure 11 shows the variation of hardness with Pb content for various Al-Pb alloys. For readers' convenience, the hardness variation in the plots is shown with varying atomic percent Pb, but calculations are done based on equivalent volume percent. Rule of mixtures line and the plot obtained from measured hardness values from microindentation tests performed with an applied load of 50 gm are also shown. Hardness values of Al and Pb used for rule of mixtures line are 1.27 GPa and 80 MPa, respectively. Experimentally measured hardness values show increasing trend initially with increasing Pb content, then a decreasing trend for larger Pb additions (Figure 11). Initial increasing hardness trend for lower Pb additions is well above the rule of mixtures, whereas the decreasing trend for higher Pb additions is nearly close to rule of mixtures. The predicted Orowan plot obtained using model equations show higher values than

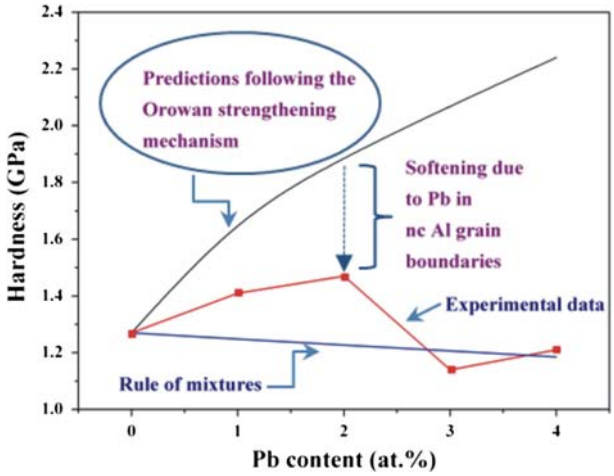

Fig. 11—Variation of hardness with Pb content obtained using Eqs. [1] and [2]. Rule of mixtures line and the plot obtained from measured hardness values (Vickers, 50 g load) are also shown.

the measured values. While calculating the Orowan plots, it is considered that the total volume of the Pb particles has equal particle size (6 nm) in all the nc Al-Pb alloys, but practically, it may not be the case and range of particle sizes could exist (Figure 9) in the overall distribution. However, the distribution is nearly uniform and significant fraction of particles is indeed in the range of 6 to 8 nm. Smaller particles and uniform distribution show influential effect on strengthening, whereas larger particles and non-uniform distribution may not show greater strengthening effect. In fact, there is a possibility that non-uniform distribution and segregation of larger second-phase particle might lead to softening of the material. It is clear from Figure 8, and Figure 9 which shows the transmission electron micrograph and the histogram of Pb particle size distribution of sintered Al-2 at. pct Pb nanocomposite that fine Pb nano particles are uniformly distributed and major fraction of which are under 10 nm. Hence, the initial increasing hardness trend observed experimentally can be attributed to the strengthening effect due to the presence of uniformly distributed Pb particles in Al matrix. No significant change in the grain size of Al matrix was observed with Pb content for various nc Al-Pb alloys, hence it is imperative that the second-phase content along with its size and distribution is solely responsible for the observed mechanical behavior.

Investigations carried out by Liu *et al.*[34] on nanostructured Al-20 wt pct Sn alloy resulted in both hardening and softening of the Al matrix. Sintering of ball-milled powders below eutectic temperature [487 K (214 °C)] resulted in homogeneous distribution of Sn in Al and sintering above eutectic temperature resulted in inhomogeneous distribution and this behavior in-turn resulted in hardening and softening effect, respectively, in nc Al-Sn system. Hence, the size and distribution of second-phase particles in the matrix greatly influence hardness of the composite. Effects of nano-sized harder "W" phase on the mechanical properties of softer Al matrix were earlier studied by Rajulapati *et al.*[35].

Hardness of Al matrix increased with increasing volume percent of W. It was observed that the hardening effect was much higher than that is expected from rule of mixtures. Based on the existing models on strengthening mechanisms in nanocrystalline materials suggested by Scattergood *et al*.,[33] the hardening effect was attributed to the Orowan-particle strengthening due to small W particles dispersed in nanocrystalline Al matrix. Recently, Atwater *et al*.[36] reported that the harder W phase enhanced the thermal stability of nanocrystalline Cu-W alloys leading to improved mechanical properties. More recent work by Varam *et al*.[37] resulted in a high hardness of 5.2 GPa and SRS of 0.025 in multi-phase nanocrystalline Al-10 at. pct W composite.

C. *Elastic Modulus Using Nanoindentation*

Elastic modulus values are calculated from reduced modulus values obtained from nanoindentation data using the following formula:[38]

$$\frac{1}{E_r} = \frac{(1 - v_i^2)}{E_i} + \frac{(1 - v_s^2)}{E_s}, \quad [3]$$

where E_r is the reduced modulus, E_i and v_i are the Young's modulus and Poisson's ratio of the diamond indenter which are considered as 1140 GPa and 0.07, respectively. v_i is the Poisson's ratio of the sample, 0.33. Nanocrystalline Al showed an average elastic modulus value of ~80 GPa which is comparable with that of conventional Al (~70 GPa). The modulus values decreased with increasing Pb addition which is usual behavior due to the low elastic modulus value of Pb. The modulus values have been reduced by ~20 to 27 pct for various Al-Pb alloys with Pb addition. The detailed compositional analysis performed using inert gas fusion technique reveals that nc Al and nc Al-4 at. pct Pb alloy had an oxygen content of 0.32 and 0.36 wt pct, respectively. Therefore, this minor oxygen content present in these samples will have very minimal effect on E as well as other mechanical properties.

This decrement in elastic modulus of various nc Al-Pb alloys could have the contribution from the presence of softer Pb phase with low elastic modulus. In the simulation work performed in Reference 23, pure Al possessed an elastic modulus in the range of 51 to 63 GPa, as the grain size is varied between 5 and 30 nm. Al-Pb alloys had an elastic modulus in the range of 50 to 56 GPa resulting in an overall reduction of nearly 10 pct with respect to pure Al. Several experimental studies showed that the elastic modulus will be decreased for nc materials in comparison to their coarse-grained counterparts especially at very finer grain sizes.[39–41] In the current study, it is experimentally found that the Pb additions resulted in the decrement of E by about 20 to 27 pct. It is to be noted that the grain size of nc Al matrix in the current study is about 53 nm whereas in Reference 23, it is 10 nm. Thus, the significant variation in E of nc Al-Pb alloys experimentally measured in the current study and theoretically calculated in Reference 23 could be because of different grain sizes employed and also the variation in different experimental conditions prevailing in experiments and simulations.

D. *Strain Rate Sensitivity and Activation Volume Studies*

Nanoindentation is a promising technique to evaluate SRS and activation volume as it offers variation of strain rate by four orders of magnitude at different peak loads.[42] SRS and activation volume studies have been carried out on different nc Al-Pb alloys by performing nanoindentation at various peak loads and loading rates. Figure 12 represents yield strength *vs* strain rate plots (on logarithmic scale) obtained from nanoindentation data for various nc Al-Pb alloys and the corresponding linear fits are also shown in Figure 12 at various peak loads. Indentations are performed at three different peak forces of 1000, 2000, and 4500 μN with loading rates of 100, 500, and 1000 μN/s for each peak force. Yield strength is calculated based on Tabor's equation,[43] $\sigma = H/3$, where H being the hardness value obtained from nanoindentation data. Loading rate divided by the peak load applied is considered as strain rate.[44,45] SRS values obtained from the slope of each plot are also shown in the plots. The yield strength values are observed to be increasing with increasing loading rate which indicates the positive SRS of these two-phase nanostructured materials.

In the current study, at room temperature, SRS values of 0.036 and 0.1 are obtained for nanocrystalline Al and Al-4 at. pct Pb, respectively. As shown in Figure 13, SRS values increased with increasing Pb content. The nanocomposite with 4 at. pct Pb showed an SRS value of 0.1 which is high for room temperature deformation conditions. It is clear from Figure 13 that the second-phase particles are definitely contributing to the enhanced SRS values which might result in improved ductility as suggested by Koch.[16] Activation volume for flow stress of these materials, assuming constant microstructure and constant temperature, can be calculated using the following relation[14]

$$v = \sqrt{3}kT\left(\frac{\partial ln\dot{\varepsilon}}{\partial \sigma}\right), \quad [4]$$

where k is the Boltzmann constant, T is the absolute temperature, $\dot{\varepsilon}$ is the strain rate, and σ *is* the yield strength. The slope of the plot of $kT\ln(\dot{\varepsilon})$ *vs* σ gives the activation volume in m^3[46] which is converted to the unit of b^3 where b is the Burgers vector of Al (0.286 nm). The calculated activation volume values (Table I) for various Al-Pb nanocomposites are much lower when compared to microcrystalline materials.

SRS data reported in the literature on various nanocrystalline materials suggests that the nc materials are rate sensitive.[47–58] Single-phase fcc materials have displayed enhanced SRS whereas the bcc materials showed reduced SRS in comparison to their respective coarse-grained counterparts. Investigations by Chinh *et al*.[53,54] on ultrafine-grained Al and Al-30 wt pct Zn alloy, revealed the possibility of obtaining improved ductility through SPD process. They observed high SRS values for these materials and suggested that enhanced

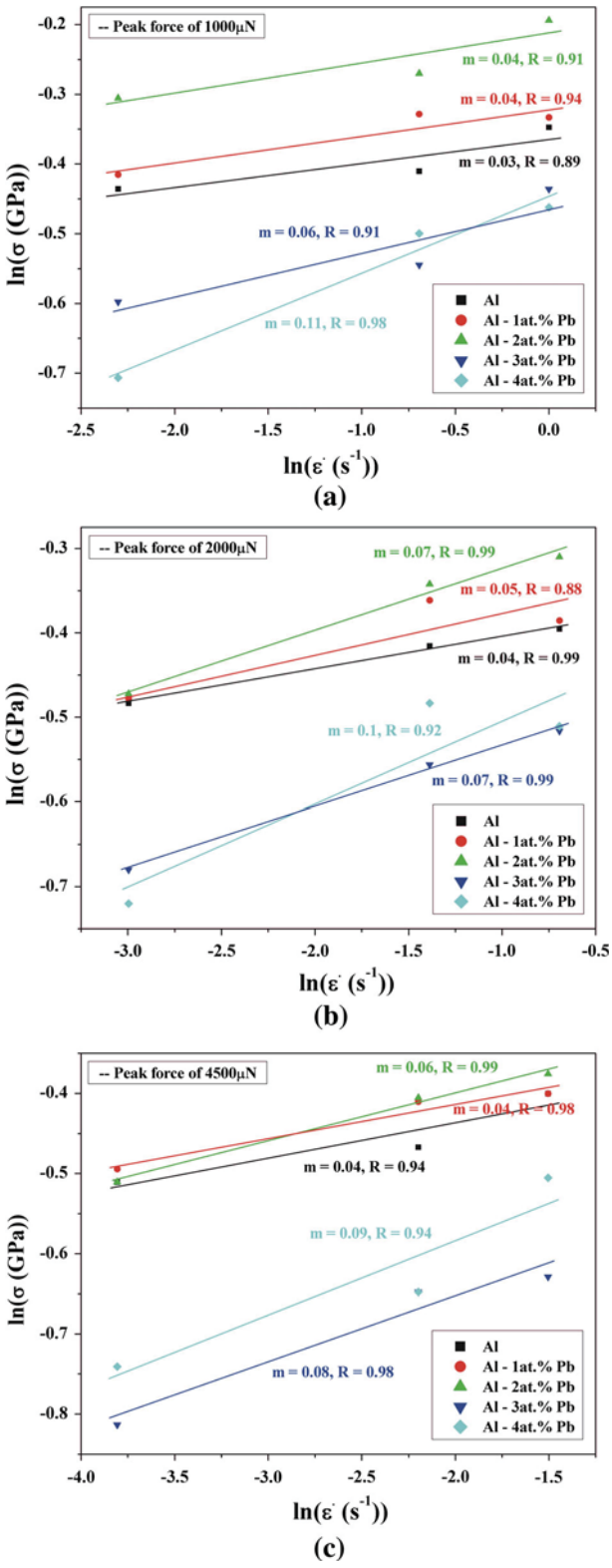

Fig. 12—Yield strength *vs* strain rate plots on logarithmic scale of Al-Pb nanocomposites at maximum peak force of (*a*) 1000 μN, (*b*) 2000 μN and (*c*) 4500 μN.

diffusion along the grain boundaries leading to grain boundary sliding resulted in increased ductility in Al-30 wt pct Zn alloy. They emphasized that there is a close relationship between increased SRS and ductility in these materials.

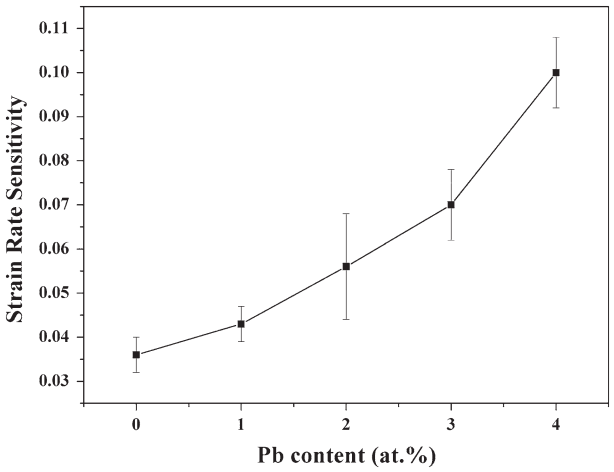

Fig. 13—Variation of strain rate sensitivity with Pb content for Al-Pb nanocomposites indicating the increase in strain rate sensitivity with increasing Pb content. The error bars indicate the variation in SRS of a given composite at various peak loads (1000 to 4500 μN).

Table I. Activation Volumes of Various Al-Pb Nanocomposites

Material	Activation Volume, υ (b^3)
Al	6.15 ± 0.62
Al-1 at. pct Pb	5.49 ± 0.72
Al-2 at. pct Pb	4.12 ± 0.41
Al-3 at. pct Pb	4.12 ± 0.26
Al-4 at. pct Pb	2.84 ± 0.13

Asaro and Suresh[14] have developed mechanistic models for activation volume and rate sensitivity and estimated increased SRS values and decreased activation volumes (3 to 10 b^3) for fcc metals. These estimated values are consistent with available experimental data. The activation volumes increased with increasing grain size. These models were based on the emission of dislocations from stress concentrations at a grain boundary or a twin boundary. Recently, Niu *et al.*,[59] studied the SRS behavior of nanostructured two-phase Cu-Cr and Cu-Zr multilayer thin films. These represent fcc-bcc and fcc-hcp combinations. In case of Cu-Cr, SRS was found to be varying between 0.022 and 0.031 whereas for Cu-Zr, SRS was in between 0.012 and 0.025. Cu-Cr had an activation volume of 11.57 to 15.20 b^3 whereas Cu-Zr had an activation volume in the range of 14.35 to 22.13 b^3. Although the single-phase bcc metals display a reduced SRS, the presence of bcc phase is not affecting the overall SRS of Cu-Cr composite in this case. This is also in agreement with our recent findings on SRS of nanocrystalline multiphase Al-10W composite[37] where the bcc $Al_{12}W$ phase did not affect the SRS of pure Al. In this work, nanostructured Al-10W composite had an SRS of 0.025 ± 0.002 and an activation volume in the range

of 1.63 to 3.88 b^3. It is to be noted that traditionally for conventional coarse-grained materials during ASTM testing procedures either strain rate jump tests or stress relaxation tests have been used. In addition, the entire microstructure is assumed to be constant during these tests.[60] In the current study, nanoindentation technique was employed to evaluate SRS and activation volume owing to the sample dimensions. Tests were performed at various peak loads and loading rates on different locations of the sample. This procedure was followed because by performing indentations at various loads and loading rates at different locations of the sample, we wanted to ensure that we are evaluating the bulk behavior of the sample to a reasonable extent possible. The reported values for SRS and activation volume for various nc Al-Pb alloys in the current study are apparent values of SRS and activation volume, respectively.

In the case of two-phase nanocrystalline materials where both matrix and second phase are having nanocrystalline (<100 nm) structural features, contribution of second phase and its crystal structure to the overall SRS of the composite material could be significant. Nanocrystalline Al-4 at. pct Pb composite had SRS of 0.1 which is almost an order of magnitude high in comparison to that of single-phase fcc metals. It is to be noted that, in the present investigation, it is fcc–fcc combination as both Al and Pb are of fcc structure.

Both SRS and activation volume are the quantitative measures for rate sensitivity of flow stress to the loading rate. In conventional coarse-grained materials with grain size around 30 to 40 μm, dislocations control the plasticity and measured activation volumes are ~1000 b^3. In all the single-phase nc materials reported so far, the measured activation volumes values are about 10 to 135 b^3. The activation volumes measured for nc Al-Pb composites in the present study are also in agreement with earlier studies and are in the range of 2.84 to 6.15 b^3, suggesting that the second phase has no influential effect on overall activation volume of two-phase nanocomposites. These low activation volumes suggest that grain boundary-mediated processes[61–63] are controlling the plastic deformation in these two-phase nanomaterials.

IV. CONCLUSIONS

A combination of high-energy ball milling and spark plasma sintering [at 573 K (300 °C)] has been used to fabricate bulk nanocrystalline two-phase Al-Pb alloys. The average grain size of the Al matrix in nc Al-2 at. pct Pb alloy is about 53 nm and Pb particles are about 6 nm in diameter. The mechanical properties are measured using both microindentation and nanoindentation. The hardness of nc Al-Pb alloys initially increases with additions up to 2 at. pct Pb and then decreases. This trend is same for both microindentation and nanoindentation studies. Hardness values obtained using microindentaion are smaller than that of nanoindentation probably due to the indention size effect. It appears that the final hardness in these nanocrystalline alloys is dictated by the competition between the Orowan particle strengthening and grain boundary weakening processes. Pb phase seems to be enhancing the SRS of nc Al-Pb alloys and the SRS increased with increasing Pb content reaching a value of 0.1 for alloy with 4 at. pct Pb. Pb present especially in the grain boundaries might be influencing the SRS *via* some grain boundary-mediated processes leading to higher SRS in the current investigation. The activation volume values for various Al-Pb alloys are in the range of 2.84 to 6.15 b^3. The enhanced SRS values and low activation volume numbers indicate that dislocations are not controlling the plasticity in these materials, instead, it is expected that the interfaces *viz*., grain boundaries and matrix/particle boundaries are the deciding factors of the deformation mechanisms.

ACKNOWLEDGMENTS

Authors are grateful to Dr. D. Chakravarty of International Advanced Research Centre for Powder Metallurgy and New Materials (ARCI), Hyderabad, India, for assisting in Spark Plasma Sintering (SPS) and Nano facility of the Indian Institute Science (IISc), Bangalore, India, for advanced TEM work. Sreedevi Varam is thankful to University Grants Commission (UGC), New Delhi, India, for providing her with Junior Research Fellowship (JRF) in Engineering and Technology. This work is supported by the Department of Science and Technology, Government of India under fast track scheme for young scientists.

REFERENCES

1. G.W. Nieman, J.R. Weertman, and R.W. Siegel: *J. Mater. Res.*, 1991, vol. 6, pp. 1012–27.
2. H. Gleiter: *Acta Mater.*, 2000, vol. 48, pp. 1–29.
3. D. Hull and D.J. Bacon: *Introduction to Dislocations*, 5th ed., Butterworth-Heinnmann, Oxford, 2011.
4. K.S. Kumar, H.V. Swygenhoven, and S. Suresh: *Acta Mater.*, 2003, vol. 51, pp. 5743–74.
5. M.A. Meyers, A. Mishra, and D.J. Benson: *Prog. Mater Sci.*, 2006, vol. 51, pp. 427–556.
6. H.V. Swygenhoven, P.M. Derlet, and A. Hsnaoui: *Phys. Rev. B*, 2002, vol. 66, pp. 024101/1–1/8.
7. V. Yamakov, D. Wolf, S.R. Phillpot, A.K. Mukherjee, and H. Gleiter: *Nat. Mater.*, 2002, vol. 1, pp. 45–48.
8. J. Schiotz, T. Vegge, F.D. Di-Tolla, and K.W. Jacobsen: *Phys. Rev. B*, 1999, vol. 60, pp. 11971–83.
9. H.V. Swygenhoven, M. Spaczer, A. Caro, and D. Farkas: *Phys. Rev. B*, 1999, vol. 60, pp. 22–25.
10. E.O. Hall: *Proc. R. Soc. (Lond.)*, 1951, vol. 64B, p. 474.
11. N.J. Petch: *J. Iron Steel Inst.*, 1953, vol. 174, pp. 25–28.
12. C.C. Koch and J. Narayan: *MRS Sym. Proc.*, 2000, vol. 634, B15. 1. 1.
13. C.C. Koch, D.G. Morris, K. Lu, and A. Inoue: *MRS Bull.*, 1999, vol. 24, pp. 54–58.
14. R.J. Asaro and S. Suresh: *Acta Mater.*, 2005, vol. 53, pp. 3369–82.
15. M.-Y. Wu and O.D. Sherby: *Scripta Metall.*, 1984, vol. 18, pp. 773–76.
16. C.C. Koch: *Scripta Mater.*, 2003, vol. 49, pp. 657–62.
17. C.C. Koch, R.O. Scattergood, and K.L. Murty: *JOM*, 2007, vol. 59, pp. 66–70.
18. B.D. Cullity: *Elements of X-ray Diffraction*, Addison-Wesley Publishing Company Inc., Reading, MA, 1956.

19. P. Scherrer: *Göttinger Nachr. Gesell*, 1918, vol. 2, pp. 98–100.
20. K.V. Rajulapati, R.O. Scattergood, K.L. Murty, G. Duscher, and C.C. Koch: *Scripta Mater.*, 2006, vol. 55, pp. 155–58.
21. H.W. Sheng, F. Zhou, Z.Q. Hu, and K. Lu: *J. Mater. Res.*, 1998, vol. 13 (2), pp. 308–15.
22. S.J. Pennycook and L.A. Boatner: *Nature*, 1988, vol. 336, pp. 565–67.
23. S. Jang, Y. Purohit, D.L. Irving, C. Padgette, D. Brenner, and R.O. Scattergood: *Acta Mater.*, 2008, vol. 56, pp. 4750–61.
24. W.D. Nix and H. Gao: *J. Mech. Phys. Solids*, 1998, vol. 46, pp. 411–25.
25. N.K. Mukhopadhyay and P. Paufler: *Int. Mater. Rev*, 2006, vol. 51 (4), pp. 209–45.
26. A.A. Elmustafa and D.S. Stone: *Acta Mater.*, 2002, vol. 50, pp. 3641–50.
27. A.A. Elmustafa and D.S. Stone: *J. Mech. Phys. Solids*, 2003, vol. 51, pp. 357–81.
28. H. Gao, Y. Huang, and W.D. Nix: *Nat. Wiss.*, 1999, vol. 86, pp. 507–15.
29. P. Paufler and B. Wolf: in *Quasicrystals*, H.-R. Trebin, ed., Wiley-VCH, Weinheim, 2003, pp. 501–22.
30. J.G. Swadener, A. Misra, R.G. Hoagland, and M. Nastasi: *Scripta Mater.*, 2002, vol. 47, pp. 343–48.
31. T.T. Zhu, X.D. Hou, A.J. Bushby, and D.J. Dunstan: *J. Phys. D: Appl. Phys.*, 2008, vol. 41, p. 074004(1-6).
32. W.W. Gerberich, N.I. Tymiak, J.C. Grunlan, M.F. Horstemeyer, and M.I. Baskes: *J. Appl. Mech.*, 2002, vol. 69, pp. 433–42.
33. R.O. Scattergood, C.C. Koch, K.L. Murty, and D. Brenner: *Mater. Sci. Eng. A*, 2008, vol. 493, pp. 3–11.
34. X. Liu, M.Q. Zeng, Y. Ma, and M. Zhu: *Mater. Sci. Eng. A*, 2009, vol. 506, pp. 1–7.
35. K.V. Rajulapati, R.O. Scattergood, K.L. Murty, Z. Horita, T.G. Langdon, and C.C. Koch: *Metall. Mater. Trans. A*, 2008, vol. 39A, pp. 2528–34.
36. M.A. Atwater, D. Roy, K.A. Darling, B.G. Butler, R.O. Scattergood, and C.C. Koch: *Mater. Sci. Eng. A*, 2012, vol. 558, pp. 226–33.
37. S. Varam, P.V.S.L. Narayana, M. Durga Prasad, D. Chakravarty, K.V. Rajulapati, and K. Bhanu Sankara Rao: Unpublished research, 2014.
38. W.C. Oliver and G.M. Pharr: *J. Mater. Res.*, 1992, vol. 7 (6), pp. 1564–83.
39. T.D. Shen, C.C. Koch, T.Y. Tsui, and G.M. Pharr: *J. Mater. Res.*, 1995, vol. 10 (11), pp. 2892–96.
40. Q. Wei, Z.L. Pan, X.L. Wu, B.E. Schuster, L.J. Kecskes, and R.Z. Valiev: *Acta Mater.*, 2011, vol. 59, pp. 2423–36.
41. Z. Pan, Y. Li, and Q. Wei: *Acta Mater.*, 2008, vol. 56, pp. 3470–80.
42. J.R. Trelewicz and C.A. Schuh: *Acta Mater.*, 2007, vol. 55, p. 5948.
43. D. Tabor: *J. Inst. Met.*, 1951, vol. 79, pp. 1–18.
44. A.C. Fisher-Cripps: *Nanoindentation*, 2nd ed., Springer, New York, 2004.
45. V. Maier, K. Durst, J. Mueller, B. Backes, H.W. Höppel, and M. Göken: *J. Mater. Res.*, 2011, vol. 26 (11), pp. 1421–30.
46. M. Ames, M. Grewer, C. Braun, and R. Birringer: *Mater. Sci. Eng. A*, 2012, vol. 546, pp. 248–57.
47. Q. Wei, S. Cheng, K.T. Ramesh, and E. Ma: *Mater. Sci. Eng. A*, 2004, vol. 381, pp. 71–79.
48. Y.T. Zhu and X. Liao: *Nat. Mater.*, 2004, vol. 3, pp. 351–52.
49. T. Zhu, J. Li, A. Samanta, H.G. Kim, and S. Suresh: *PNAS*, 2007, vol. 104 (9), pp. 3031–36.
50. R. Schwaiger, B. Moser, M. Dao, N. Chollacoop, and S. Suresh: *Acta Mater.*, 2003, vol. 51, pp. 5159–72.
51. J. May, H.W. Höppel, and M. Göken: *Scripta Mater.*, 2005, vol. 53, pp. 189–94.
52. B. Ahn, R. Mitra, A.M. Hodge, E.J. Lavernia, and S.R. Nutt: *Mater. Sci. Forum*, 2008, vols. 584–586, pp. 221–26.
53. N.Q. Chinh, T. Csanádi, J. Gubicza, R.Z. Valiev, B.B. Straumal, and T.G. Langdon: *Mater. Sci. Forum*, 2011, vols. 667–669, pp. 677–82.
54. N.Q. Chinh, T. Csanádi, T. Győri, R.Z. Valiev, B.B. Straumal, M. Kawasaki, and T.G. Langdon: *Mater. Sci. Eng. A*, 2012, vol. 543, pp. 117–20.
55. Y.M. Wang and E. Ma: *Mater. Sci. Eng. A*, 2004, vols. 375–377, pp. 46–52.
56. Q. Wei: *J. Mater. Sci.*, 2007, vol. 42, pp. 1709–27.
57. X.Z. Liao, F. Zhou, E.J. Lavernia, D.W. He, and Y.T. Zhu: *Appl. Phys. Lett.*, 2003, vol. 83, pp. 5062–64.
58. M. Chen, E. Ma, K.J. Hemker, H. Sheng, Y. Wang, and X. Cheng: *Science*, 2003, vol. 300, pp. 1275–77.
59. J.J. Niu, J.Y. Zhang, G. Liu, P. Zhang, S.Y. Lei, G.J. Zhang, and J. Sun: *Acta Mater.*, 2012, vol. 60, pp. 3677–89.
60. U.F. Kocks, A.S. Argon, and M.F. Ashby: *Progress in Materials Science*, Pergamon Press, Oxford, 1975, p. 129.
61. X.Z. Liao, F. Zhou, E.J. Lavernia, S.G. Srinivasan, M.I. Baskes, D.W. He, and Y.T. Zhu: *Appl. Phys. Lett.*, 2003, vol. 83 (4), pp. 632–34.
62. Z. Shan, E.A. Stach, J.M.K. Wiezorek, J.A. Knapp, D.M. Follstaedt, and S.X. Mao: *Science*, 2004, vol. 305, pp. 654–56.
63. H.V. Swygenhoven and J.R. Weertman: *Mater. Today*, 2006, vol. 9 (5), pp. 24–31.